Received: 9 June 2023 | Revised: 29 February 2024 | Accepted: 4 May 2024

DOI: 10.33012/navi.651

ORIGINAL ARTICLE

Array-Aided Precise Orbit and Attitude Determination of CubeSats using GNSS

Amir Allahvirdi-Zadeh[1] | **Ahmed El-Mowafy**[1]

[1] School of Earth and Planetary Sciences, Curtin University, GPO Box U1987, Perth, Western Australia 6845

Correspondence
Amir Allahvirdi-Zadeh
School of Earth and Planetary Sciences, Curtin University, GPO Box U1987, Perth, Western Australia 6845.
Email: amir.allahvirdizadeh@curtin.edu.au

Abstract

CubeSats hold promise for various applications, but their viability in demanding missions such as future low Earth orbiting position, navigation, and timing (LEO-PNT) systems hinges on higher orbital accuracy and reliable attitude information. To address these challenges, we present an array-aided combined precise orbit and attitude determination model with an optimal solution. In the estimation process, multi- and affine-constrained models are used to precisely determine the attitude, and then, highly precise observations for an antenna array are reconstructed based on fixed ambiguities and a decorrelation step. Validations confirm the significance of integer ambiguities in the model, highlighting the cost-effectiveness of this model compared with star trackers for attitude determination. The reconstructed observations outperform the original observations, leading to improved orbital components, with the three-dimensional root mean square (RMS) equal to 4.1 cm. The observation residuals are smoother, with an RMS of 6 mm, half of that obtained via a single antenna. The developed models offer great potential for CubeSats, advancing their orbit and attitude determination capabilities.

Keywords

array-aided positioning, CubeSats, LEO-PNT, MC-LAMBDA, precise attitude determination, precise orbit determination

1 | INTRODUCTION

Small low Earth orbiting (LEO) satellites, particularly CubeSats, are becoming increasingly favored among industry and research institutes, primarily because of their relatively low-cost components, simpler design and building procedures, and the possibility of mass production and launching. Precise orbit determination (POD) of CubeSats is generally performed using two well-known methods: kinematic and reduced-dynamic POD (Allahvirdi-Zadeh, Wang, & El-Mowafy, 2022). POD is mainly affected by the performance of onboard sensors, the number of observations from the global navigation satellite system (GNSS), and deficiencies in the applied dynamic models. When considering real-time or onboard POD for CubeSats, it is also crucial to account for other factors, including the availability of observations, precise corrections, and limitations in onboard power and

processing units. Several studies have investigated the impact of such factors on POD. For example, Wang et al. (2020) explored the influence of observation interruptions on POD caused by limited onboard power in small satellites. The authors reached an orbital accuracy of several centimeters in the post-processing mode. Hauschild & Montenbruck (2021) demonstrated significant improvement in onboard POD accuracy by incorporating additional GNSSs such as Galileo and BeiDou-3 alongside Global Positioning System (GPS) observations, utilizing GNSS broadcast ephemeris. Allahvirdi-Zadeh et al. (2021) highlighted the availability of precise corrections via space links through the Australian Satellite-Based Augmentation System and the Japanese Quasi-Zenith Satellite System, which improve the accuracy of onboard POD from several decimeters in the case of using broadcast ephemeris to several centimeters, primarily depending on the quality of the utilized space links. This approach holds promise for future applications requiring real-time precise orbital components. Palomo et al. (2019) extended the concept of autonomous onboard POD by designing a low-cost receiver for CubeSats based on software-defined radio (SDR) and an integrated field programmable gate array. Allahvirdi-Zadeh et al. (2022) proposed a practical weighting function to handle onboard GNSS observations collected by CubeSats to improve the performance of CubeSat POD in the validation steps. They also investigated the concept of utilizing precise inter-satellite ranges in onboard POD for a CubeSat constellation. The authors achieved improvements of 1–3 dm in the orbital accuracy of the deputy CubeSat compared with nominal onboard POD (Allahvirdi-Zadeh & El-Mowafy, 2022b). Such a level of accuracy for CubeSat POD has also been confirmed by Arnold et al. (2023).

The aforementioned studies have demonstrated that CubeSats have the capability to deliver highly accurate orbital information, with accuracies primarily ranging from a few centimeters for post-processing mode using extensive dynamic models to several decimeters for onboard POD. These orbital accuracies are essential for a wide range of applications. However, there remains a question regarding their suitability for applications that demand even higher levels of accuracy, such as emerging LEO position, navigation, and timing (PNT) systems (Li et al., 2019; Jiang et al., 2021; El-Mowafy et al., 2022). In addition to accurate orbital information, key requirements for successful PNT from CubeSats include stable, reliable onboard clocks, strong navigation signals with high integrity, the presence of inter-satellite links, compensation for atmospheric delays, and integration with other GNSSs.

Numerous studies are being conducted on the viability of utilizing LEO satellites for PNT, either as a standalone navigation system or as an augmentation to an existing GNSS. However, both scenarios present the challenge of deploying a constellation comprising numerous large, intricate, and costly LEO satellites. Meanwhile, the utilization of low-cost CubeSats is theoretically feasible and could offer a more economical solution. Nonetheless, one crucial requirement for CubeSats is the maintenance of highly precise orbits. To this end, this study aims to provide a new method for improving the orbital accuracy of CubeSats.

In addition to POD, precisely determining satellite attitude is another essential requirement for both LEO-PNT systems (Allahvirdi-Zadeh, El-Mowafy, & Wang, 2024; Allahvirdi-Zadeh, El-Mowafy, Mcclusky et al., 2024) and specific pointing operations, such as aligning solar panels with the sun, orienting a downlink antenna toward ground stations, or directing sensors toward specific objects. Attitude information also plays a crucial role in various stages of POD, such as in estimating the phase wind-up effect, applying antenna sensor offsets, and modeling phase center offsets and variations.

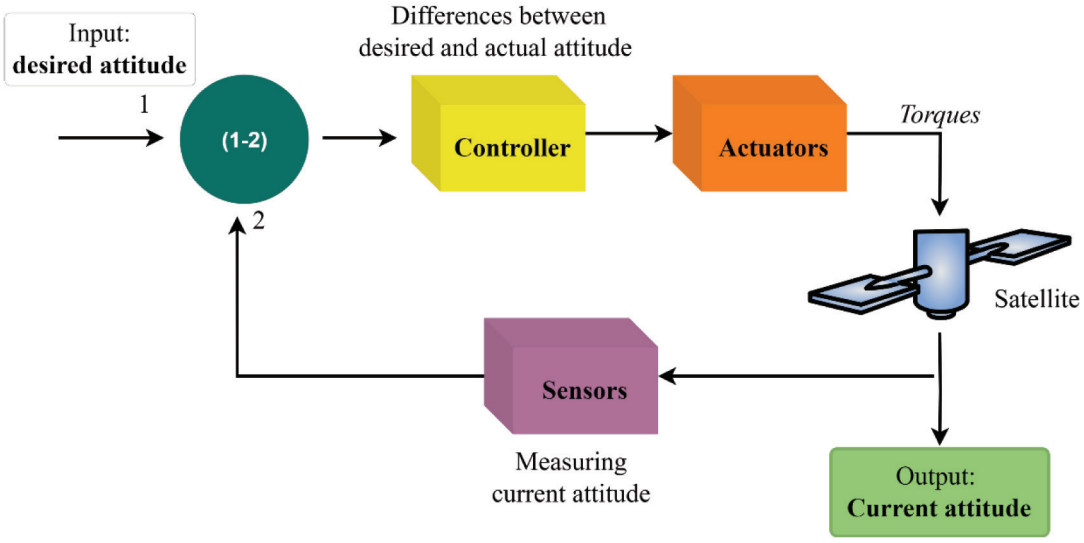

FIGURE 1 Closed-loop ADCS

A satellite's attitude is determined and controlled by the attitude determination and control system (ADCS), which is part of the satellite's bus component. The ADCS is based on determining the angular rotations (roll, pitch, and yaw angles) with respect to the satellite reference frame (SRF) or their equivalent quaternions. The actuators control the rotation of attitude angles to produce the torques necessary to rotate the satellite to the desired attitude state. A simple structure of such a closed-loop ADCS is shown in Figure 1.

Various sensors within the ADCS can measure a CubeSat's attitude, including sun sensors, magnetometers, and star trackers. Sun sensors use the sun's direction with respect to the SRF to provide attitude information. However, these sensors only work in sunlight, reducing their applicability when the satellite crosses a shadow region. In contrast, magnetometers measure the direction and strength of the Earth's magnetic field and compare this information with a high-fidelity model of the Earth's field to determine the attitude. However, magnetometers provide lower accuracy than other sensors. Star trackers determine attitude by capturing available stars and comparing them with accurate maps of the brightest stars stored in the satellite's memory. Similar to sun sensors, star trackers can only provide attitude information in two dimensions. Therefore, more than one sensor is required to obtain three-dimensional (3D) attitude information. Table 1 provides the specifications of highly accurate attitude determination sensors currently available for CubeSats. Equipping CubeSats with highly accurate star trackers can be expensive, especially in the case of launching a constellation such as Spire (https://spire.com). Consequently, CubeSat providers often combine relatively inexpensive sensors such as magnetometers and sun sensors in the ADCS to perform attitude determination, sacrificing final accuracy.

An alternative method for attitude determination involves equipping a satellite with more than one GNSS antenna and applying a differential technique to eliminate common errors and determine the satellite's attitude. According to personal communication with CubeSat developers, the cost of a patch GNSS antenna for a CubeSat is less than 1500 USD. This antenna is approximately 2×2 cm^2 and weighs less than 40 g. Considering these specifications, an array of 3–4 antennas would be a more cost-effective option than the available sensors listed in Table 1. Furthermore, this array would also meet the dimension and weight restrictions of most CubeSats.

TABLE 1
Specifications of ADCS Sensors for CubeSats (Source: https://www.cubesatshop.com/)

Name	Sensor Type	Accuracy (1σ)	Power (W)	Weight (g)	Cost (USD)
Sagitta	Star tracker	2 arc seconds	<1.4	275	~45000
Twinkle	Star tracker	15 arc seconds	<0.6	40	~45000
NSS	Magnetometer	1°	<0.7	85	~15000
NSS	Sun sensor	<0.5°–0.1°	<0.013	5–35	~12000

The concept of array-based attitude determination was developed more than three decades ago for the RADCAL mission (Cohen, Lightsey et al., 1994) and has been applied in various space missions (Cohen, Parkinson et al., 1994; Freesland et al., 1996; Unwin et al., 2002; Gomez, 2005; Hauschild et al., 2020; Jin et al., 2022). The concept was further extended to fully exploit the antenna geometry and integer ambiguities, resulting in the development of the constrained and multi-constrained least-squares ambiguity decorrelation adjustment methods (C-LAMBDA and MC-LAMBDA) (Teunissen, 2007, 2008, 2010). This solution has been evaluated for attitude determination of ground, maritime, and aeronautics platforms (Giorgi et al., 2011; Giorgi, Teunissen, & Gourlay, 2012; Giorgi, Teunissen, Verhagen, & Buist, 2012; Nadarajah et al., 2012; Nadarajah et al., 2013; Nadarajah & Teunissen, 2014; Nadarajah et al., 2014; Nadarajah et al., 2016). In our previous research, we conducted an evaluation of array-based attitude determination methods specifically designed for CubeSats and achieved a precision of 0.06°–0.13° for the fixed attitude angles (Allahvirdi-Zadeh & El-Mowafy, 2022a). In this contribution, our objective extends to developing an optimal solution for both orbit and attitude determination.

Teunissen developed the concept of array-aided precise point positioning (A-PPP) (Teunissen, 2012b) to exploit the aforementioned constraints and to improve the combined PPP and attitude determination problem. The concept of A-PPP and attitude determination has also been extended to the joint relative positioning and attitude determination model (Wu et al., 2020). In this study, we exploit the array-aided positioning and multi-constrained attitude determination concepts to develop a combined model. This model enhances the accuracy of estimated orbits and facilitates precise attitude determination for CubeSats equipped with limited power and low-quality sensors. This approach is particularly valuable for real-time applications, including LEO-PNT systems, where simultaneous and accurate determination of both attitude and orbit is essential. In the following sections, and given the absence of an actual antenna array onboard a CubeSat, we conduct an extensive reduced-dynamic POD for an operational CubeSat. Subsequently, we utilize these highly accurate orbits to simulate an antenna array comprising four antennas for a 12U CubeSat. Through comprehensive testing scenarios, we validate the efficacy of the proposed model.

2 | COMBINED ARRAY-AIDED PRECISE ORBIT AND ATTITUDE DETERMINATION MODEL

In this section, a combined array-aided model for precise orbit and attitude determination is developed. The sizes of the main matrices defined here are given in Table A-1 in the Appendix. The sizes of the remaining matrices can be computed via linear algebra.

Let us begin by forming a vectorial representation of the inter-satellite single-differenced (SD) code and phase observations $\left(P_r=\left[p_{r,1}^T,\cdots,p_{r,f}^T\right],\ \Phi_r=\left[\varphi_{r,1}^T,\cdots,\varphi_{r,f}^T\right]\right)$ for frequencies 1 to f. These observations are obtained from satellites 1 to m, collected by arbitrary onboard antennae r. Considering $p_{r,f}=\left[p_{r,f}^{1s},\cdots,p_{r,f}^{ms}\right]^T$ and $\varphi_{r,f}=\left[\varphi_{r,f}^{1s},\cdots,\varphi_{r,f}^{ms}\right]^T$ for arbitrary frequency f, where s serves as the reference GNSS satellite, we have the following model:

$$\begin{aligned}E(P_r)&=\left(e_f^T\otimes\left[\left(g_r^{1s}\right)^T,\cdots,\left(g_r^{ms}\right)^T\right]^T\right)b_r+\left(\left[\mu_1,\cdots,\mu_f\right]^T\otimes \mathrm{I}_{m-1}\right)i_r+\varepsilon_{P_r}\\ E(\Phi_r)&=\left(e_f^T\otimes\left[\left(g_r^{1s}\right)^T,\cdots,\left(g_r^{ms}\right)^T\right]^T\right)b_r-\left(\left[\mu_1,\cdots,\mu_f\right]^T\otimes \mathrm{I}_{m-1}\right)i_r\\ &\quad+\left(diag\left[\lambda_1,\cdots,\lambda_f\right]\otimes \mathrm{I}_{m-1}\right)z_r+\varepsilon_{\Phi_r}\end{aligned}\tag{1}$$

Here, $E(.)$ represents the expected value, and $\otimes$ indicates the Kronecker product (Schott, 2016). $e_f=\left[1,\cdots,1\right]_{1\times f}$, and $g_r^{is}=\frac{x^s(t-\tau_r^s)-x_r(t)}{\left\|x^s(t-\tau_r^s)-x_r(t)\right\|}-\frac{x^i(t-\tau_1^i)-x_r(t)}{\left\|x^i(t-\tau_1^i)-x_r(t)\right\|}$ contains the difference of unit vectors to satellites i and s (for $i=1,\ldots,m$). This term is computed by using the orbital vectors of GNSS satellites (x^s and x^i) at the time of transmission $(t-\tau)$ and the antenna coordinates (x_r) at the time of reception (t) of the signals, considering τ as the signal travel time for each observation. b_r contains the unknown orbital components of the CubeSat in the Earth-centered, Earth-fixed (ECEF) coordinate system. $\mu_f=\left(\frac{\lambda_f}{\lambda_1}\right)^2$ is the ionospheric coefficient for frequency f, where λ_f indicates the wavelength of that frequency. I_{m-1} is the identity matrix with size $m-1$. $i_r=\left[i_r^{1s},\cdots,i_r^{ms}\right]^T$ and $z_r=\left[n_r^{1s},\cdots,n_r^{ms}\right]^T$ denote SD ionospheric delays and phase ambiguities, respectively. To obtain a more compact model, we include the SD observations in $y_r=\left[P_r,\Phi_r\right]^T$ and define $G_r=e_{2f}^T\otimes\left[g_r^{1s^T},\cdots,g_r^{ms^T}\right]$ and $A=\left[0^T,\Lambda^T\right]\otimes \mathrm{I}_{m-1}$, where $\Lambda=diag\left[\lambda_1,\cdots,\lambda_f\right]$ and $d_r=\left[\left(\left([\mu_1,\cdots,\mu_f]^T\otimes \mathrm{I}_{m-1}\right)i_r+\varepsilon_{P_r}\right)^T,\left(-\left([\mu_1,\cdots,\mu_f]^T\otimes \mathrm{I}_{m-1}\right)i_r+\varepsilon_{P_r}\right)^T\right]^T$. The GNSS observation model is then expressed as follows:

$$E(y_r)=Az_r+G_rb_r+d_r\tag{2}$$

Now, let us consider an array of a antennae onboard a CubeSat. For attitude determination, the vectorial form of the linearized double-differenced (DD) GNSS observations between each arbitrary pair of antennae 1 and 2 can be formulated as follows:

$$\begin{aligned}E\left(p_{12}^{1s}\right)&=\rho_{12}^{1s}\\ E\left(\varphi_{12}^{1s}\right)&=\rho_{12}^{1s}+\lambda n_{12}^{1s}\end{aligned}\tag{3}$$

where $n_{12}^{1s}=n_2^{1s}-n_1^{1s}$ is the DD ambiguity and ρ_{12}^{1s} is defined as follows:

$$\begin{aligned}\rho_{12}^{1s}&=\rho_1^1\left(t-\tau_1^1(t),t\right)-\rho_1^s\left(t-\tau_1^s(t),t\right)+\rho_2^s\left(t-\tau_2^s(t),t\right)-\rho_2^1\left(t-\tau_2^1(t),t\right)\\ &=\left\|x^1\left(t-\tau_1^1\right)-x_1(t)\right\|-\left\|x^s\left(t-\tau_1^s\right)-x_1(t)\right\|+\left\|x^s\left(t-\tau_2^s\right)-x_2(t)\right\|-\left\|x^1\left(t-\tau_2^1\right)-x_2(t)\right\|\end{aligned}\tag{4}$$

which can be replaced by denoting the baseline vector as b_{12} and defining $x_1(t) = x_2(t) + b_{12}$ as follows:

$$\begin{aligned}\rho_{12}^{1s}\left(b_{12},t\right) = &\left\|x^1\left(t-\tau_1^1\right)-x_2\left(t\right)-b_{12}\right\| - \left\|x^s\left(t-\tau_1^s\right)-x_2\left(t\right)-b_{12}\right\| \\ &+\left\|x^s\left(t-\tau_2^s\right)-x_2\left(t\right)\right\| - \left\|x^1\left(t-\tau_2^1\right)-x_2\left(t\right)\right\|\end{aligned} \tag{5}$$

To linearize Equation (5), a Taylor series expansion is applied at $b_{12} = 0$ as follows:

$$\rho_{12}^{1s}\left(b_{12},t\right) = \rho_{12}^{1s}\left(0,t\right) + \left(\frac{x^1\left(t-\tau_1^1\right)-x_2\left(t\right)}{\left\|x^1\left(t-\tau_1^1\right)-x_2\left(t\right)\right\|}\right)^T b_{12} + \left(\frac{x^s\left(t-\tau_1^s\right)-x_2\left(t\right)}{\left\|x^s\left(t-\tau_1^s\right)-x_2\left(t\right)\right\|}\right)^T b_{12} \tag{6}$$

Finally, by defining $\Delta P_{12}^{1s} = p_{12}^{1s}(t) - p_{12}^{1s}(0,t)$ and $\Delta\Phi_{12}^{1s} = \varphi_{12}^{1s}(t) - \varphi_{12}^{1s}(0,t)$ and forming the geometry component of the design matrix as $g_{12}^{1s} = \frac{x^s(t-\tau_1^s)-x_2(t)}{\left\|x^s(t-\tau_1^s)-x_2(t)\right\|} - \frac{x^1(t-\tau_1^1)-x_2(t)}{\left\|x^1(t-\tau_1^1)-x_2(t)\right\|}$, we obtain the following vectorial forms of the linearized DD GNSS observations:

$$\begin{aligned}E\left(y_{P_{12}}\right) &= \left(e_f^T \otimes G_{12}\right) b_{12} \\ E\left(y_{\Phi_{12}}\right) &= \left(e_f^T \otimes G_{12}\right) b_{12} + \left(\Lambda \otimes \mathrm{I}_{m-1}\right) N_{12}\end{aligned} \tag{7}$$

where $y_{P_{12}} = \left[\Delta P_{12}^{1s}, \cdots, \Delta P_{12}^{ms}\right]^T$, $y_{\Phi_{12}} = \left[\Delta\Phi_{12}^{1s}, \cdots, \Delta\Phi_{12}^{ms}\right]^T$, and $G_{12} = \left[g_{12}^{1s}, \cdots, g_{12}^{ms}\right]^T$. The matrix $N_{12} = \left[n_{12}^{1s}, \cdots, n_{12}^{ms}\right]^T$ comprises the DD ambiguities, transformed to range via multiplication by the frequency wavelength. Note that the elements of G_{12} are similar to those of G_r.

It is assumed that the covariance matrices of undifferenced observations are $Q_p = \sigma_p^2 C$ and $Q_\varphi = \sigma_\varphi^2 C$, which are formed by multiplying the standard deviation σ by the cofactor matrix C computed from elevation-angle-based or SNR-based weighting functions (Allahvirdi-Zadeh & El-Mowafy, 2021). By considering the DD operator as $\nabla = \left[-e_{m-1}^T, \mathrm{I}_{m-1}\right] \times \left(\mathrm{I}_m \otimes [-1, 1]\right)$, combining the undifferenced observations of the two antennae as $p_{1,2} = \left[p_1^1, p_2^1, \cdots, p_1^m, p_2^m\right]^T$ and $\varphi_{1,2} = \left[\varphi_1^1, \varphi_2^1, \cdots, \varphi_1^m, \varphi_2^m\right]^T$, and expressing the covariance matrices of these observations as $Q_{p_{1,2}} = Q_p \otimes I_2$ and $Q_{\varphi_{1,2}} = Q_\varphi \otimes I_2$, we obtain the following for the covariance matrices of the DD observables of the two antennae:

$$\begin{aligned}Q_{y_{P_{12}}} &= \nabla Q_{p_{1,2}} \nabla^T \\ Q_{y_{\Phi_{12}}} &= \nabla Q_{\varphi_{1,2}} \nabla^T\end{aligned} \tag{8}$$

The next step is to collect all DD observations and ambiguities of all of the baselines in $Y = \left[(y_{P_{12}})^T, \cdots, (y_{P_{1(a-1)}})^T, (y_{\Phi_{12}})^T, \cdots, (y_{\Phi_{1(a-1)}})^T\right]^T$ and $Z = \left[(N_{12})^T, \cdots, (N_{1(a-1)})^T\right]^T$. We then define $A = \left[0^T, \Lambda^T\right]^T \otimes I_{m-1}$ and $G = e_{2f}^T \otimes G_{12}$ to link the DD data to the ambiguities and geometry of the satellites. Utilizing the multivariate Gauss–Markov equation and arranging the baselines in matrix

$B=\left[b_{12},\cdots,b_{1(a-1)}\right]$, we derive the following multivariate formulation of the model for determining the attitude of the CubeSat:

$$E(Y)=AZ+GB \tag{9}$$

There are two critical points to consider in this model:

1. Because of the small size of CubeSats (typically 10×10×10 cm^3 per unit), the onboard antennae are mounted very close to each other. Therefore, the unit line-of-sight vectors to the same satellites are considered identical, giving a negligible error. Hence, $G_{12}=G_{13}=\ldots=G_{1(a-1)}=G_r$.
2. The unknown parameters are DD ambiguities in Z and baselines in B. Because the array geometry is known in the SRF as B_0, an estimation of the baselines will enable us to determine the CubeSat attitude by applying the attitude matrix R as $B=RB_0$. This attitude matrix is used to transform the SRF to the ECEF frame and can be expressed by using rotation angles or quaternions.

To further strengthen the model and fully exploit the known geometry of the baselines, the two following constraints are applied:

- The DD ambiguities are integers ($Z\in\mathbf{Z}^{f(m-1)\times(a-1)}$, where a is the total number of antennae in the array).
- This attitude matrix is orthonormal ($R^TR=\mathrm{I}\quad R\in O^{3\times q}$, where q is the number of unknown baselines).

The first constraint ensures that highly accurate phase observations are used, which, in turn, enable precise orbit and attitude determination for CubeSats. The second constraint provides increased reliability in the estimation by enabling a higher success rate in determining the ambiguities compared with the unconstrained model.

Taking Equations (2) and (9) with the aforementioned constraints and using the *vec* operator to transform the $m\times n$ matrix into an *mn*-sized vector, we can define the following combined multivariate constrained orbit and attitude determination model for CubeSats, called the *array-aided precise orbit and attitude determination (A-POAD) model*:

$$\left.\begin{aligned}E(y_r)&=Az_r+Gb_r+d_r\\E(Y)&=AZ+GRB_0\end{aligned}\right\}\Rightarrow$$
$$E\left(vec\left[y_r,Y\right]\right)=vec\left(A\left[z_r,Z\right]+G\left[b_r,RB_0\right]+\left[d_r,0\right]\right),\quad Z\in\mathbf{Z}^{f(m-1)\times(a-1)},\quad R\in O^{3\times q} \tag{10}$$

In A-POAD, two distinct models for the orbit and attitude determination of CubeSats are combined; each can be solved independently. However, as explained below, correlations exist between observations in the combined model, which should be taken into account. Otherwise, the optimality of the solution will be reduced.

The observation set in the A-POAD model is reached from the SD observations by using the following equation (Li & Teunissen, 2014):

$$vec\left[y_r,Y\right]=\left(\left[c_1^T,D_{a-1}^T\right]\otimes\mathrm{I}_{2f(m-1)}\right)vec(Y_r) \tag{11}$$

where $c_1 = \left[1, 0, \cdots, 0\right]^T$, $D_{a-1}^T = \left[-e_{a-1}, \mathrm{I}_{a-1}\right]$ is the differencing matrix and $Y_r = \left[y_1, \cdots, y_a\right]$. The covariance matrix of the A-POAD observations is calculated by applying the error propagation law to Equation (11) as follows:

$$\begin{aligned} Q_{vec\left[y_r, Y\right]} &= \left(\left[c_1^T, D_{a-1}^T\right] \otimes \mathrm{I}_{2f(m-1)}\right) Q_{vec(Y_r)} \left(\left[c_1, D_{a-1}\right] \otimes \mathrm{I}_{2f(m-1)}\right) \\ &= Q_r \otimes \left(Q_f \otimes blkd\left[D_{m-1} Q_p D_{m-1}^T, D_{m-1} Q_\varphi D_{m-1}^T\right]\right) \end{aligned} \tag{12}$$

where $Q_r = \begin{bmatrix} c_1^T Q_a c_1 & c_1^T Q_a D_{a-1}^T \\ D_{a-1} Q_a c_1 & D_{a-1} Q_a D_{a-1}^T \end{bmatrix}$ indicates the precision contribution of the antenna, Q_a is the covariance matrix of the array, Q_f is the contribution of the frequencies, and the matrices Q_p and Q_φ represent the undifferenced code and phase precision contributions, respectively. The term *blkd* indicates the block-diagonal matrix. Equation (12) includes non-diagonal values that indicate the correlation between the two sets of observations (y_r and Y) in our combined model.

To obtain a rigorous solution for the A-POAD model, the observations are decorrelated via the invertible decorrelating transformation defined by Teunissen (2012b) as follows:

$$\begin{aligned} &vec\left[\bar{y}, Y\right] \\ &= \left(\begin{bmatrix} 1 & -c_1^T Q_r D_{a-1}^T \left(D_{a-1} Q_r D_{a-1}^T\right)^{-1} \\ 0_{a-1} & \mathrm{I}_{a-1} \end{bmatrix} \otimes \mathrm{I}_{2f(m-1)}\right) vec\left(A\left[z_r, Z\right] + G\left[b_r, RB_0\right] + \left[d_r, 0\right]\right) \end{aligned} \tag{13}$$

Finally, we obtain the following decorrelated A-POAD model:

$$\begin{aligned} &E\left(vec\left[\bar{y}, Y\right]\right) = vec\left(A\left[\bar{z}, Z\right] + G\left[\bar{b}, RB_0\right] + \left[d_r, 0\right]\right), \quad Z \in \mathbf{Z}^{f(m-1)\times(a-1)}, \quad R \in O^{3\times q} \\ &Q_{vec\left[\bar{y}, Y\right]} = blkd\left[\left(e_a\, Q_r^{-1}\, e_a^T\right)^{-1}, D_{a-1} Q_r D_{a-1}^T\right] \otimes \left(Q_f \otimes blkd\left[D_{m-1} Q_p D_{m-1}^T, D_{m-1} Q_\varphi D_{m-1}^T\right]\right) \end{aligned} \tag{14}$$

where the decorrelated observations are derived from $\bar{y} = y_r - Y\left(D_{a-1} Q_r D_{a-1}^T\right)^{-1} D_{a-1} Q_r c_1$ and the combined weighted least-squares solution of all antenna positions is $\bar{b} = b_r - B(D_{a-1} Q_r D_{a-1}^T)^{-1} D_{a-1} Q_r c_1$. The covariance matrix of the observations in Equation (14) is a block-diagonal matrix, confirming that the observations of the A-POAD model are now decorrelated. For a proof of the covariance matrix calculation, see the work by Teunissen (2012b) and Li & Teunissen (2014).

We can now obtain a robust solution, which is achieved by dividing the A-POAD model into two distinct components: 1) *array-aided precise orbit determination (A-POD)* and 2) *array-aided precise attitude determination (A-PAD)*. These two components can be solved independently, allowing us to effectively leverage the entire covariance matrix of the observations in the A-POD component. According to Teunissen (2012b), it has been proven that the decorrelated observations $\bar{y}$ have smaller variances than the original observations. The new variance is proportional to the number of antennae in the array as $\mathrm{var}(\bar{y}) = \frac{1}{a}\mathrm{var}(y_r)$. This theoretical insight also validates the improvement of POD achieved by using the array-aided concept.

The first component of our solution is the A-POD model, defined as follows:

$$\begin{aligned} E\left(\bar{y}\right) &= A\bar{z} + G\bar{b} + d_r \\ Q_{\bar{y}} &= \left(e_a\, Q_r^{-1}\, e_a^T\right)^{-1} \otimes \left(Q_f \otimes blkd\left[D_{m-1} Q_p D_{m-1}^T, D_{m-1} Q_\varphi D_{m-1}^T\right]\right) \end{aligned} \tag{15}$$

We can have two solutions for this A-POD model:

1. A-POD solution without integer ambiguities: In this scenario, the focus is solely on reconstructing the A-POD observations using Y. When the antenna configuration is symmetrical, the A-POD model provides observations of the center of gravity of the antenna array. It is worth noting again that these observations have improved accuracy compared with the primary POD observations, as discussed above. This improved accuracy is particularly valuable for CubeSats equipped with commercial off-the-shelf (COTS) sensors and GNSS receivers, which generally exhibit higher noise levels than the advanced ADCSs employed in larger LEO satellites. The impact of these noise sources on POD outputs was investigated in our earlier work (Allahvirdi-Zadeh, Awange et al., 2022).
2. A-POD solution with integer ambiguities: In this case, we initially utilize observations Y to reconstruct the A-POD observations. Subsequently, we employ Z to address the integer ambiguities within the following A-POD observations:

$$\bar{\bar{y}} = \bar{y} + AZ\left(D_{a-1}Q_rD_{a-1}^T\right)^{-1}D_{a-1}Q_rc_1 \tag{16}$$

$\bar{\bar{y}}$ indicates the observations with fixed integer ambiguities, highlighting the effectiveness and benefit of our A-POD model. It is important to emphasize that the integer ambiguities are the output of the A-PAD model, which is defined and discussed in detail below.

The second component of our solution is the following multi-constrained A-PAD model:

$$\begin{aligned} E(Y) &= AZ + GRB_0, \qquad Z \in \mathbf{Z}^{f(m-1)\times(a-1)}, \qquad R \in O^{3\times q} \\ Q_Y &= D_{a-1}Q_rD_{a-1}^T \otimes \left(Q_f \otimes blkd\left[D_{\boldsymbol{m}-1}Q_pD_{m-1}^T, D_{m-1}Q_\varphi D_{m-1}^T\right]\right) \end{aligned} \tag{17}$$

The solution for this model is obtained in two steps. First, we solve the least-squares normal equation to obtain the unconstrained float estimations for ambiguities $\hat{Z}$ and attitude $\hat{R}$:

$$\begin{bmatrix} vec(\hat{Z}) \\ vec(\hat{R}) \end{bmatrix} = \left(\begin{bmatrix} I_{a-1} \otimes A^T \\ B_0 \otimes G^T \end{bmatrix} Q_Y^{-1}\begin{bmatrix} I_{a-1} \otimes A & B_0^T \otimes G \end{bmatrix}\right)^{-1}\begin{bmatrix} I_{a-1} \otimes A^T \\ B_0 \otimes G^T \end{bmatrix} Q_Y^{-1}vec(Y) \tag{18}$$

Second, we solve the following minimization problem while considering the aforementioned constraints:

$$\begin{aligned} \min_{\substack{Z\in\mathbf{Z}^{m\times 2} \\ R\in O^{3\times 2}}} \left\|vec\left(Y - AZ - GRB_0\right)\right\|^2 &= \left\|vec\left(Y - A\hat{Z} - G\hat{R}B_0\right)\right\|_{Q_Y}^2 + \\ &\underbrace{\min_{Z\in\mathbf{Z}^{f(m-1)\times(a-1)}}\left(\left\|vec\left(\hat{Z}-Z\right)\right\|_{Q_{\hat{Z}}} + \min_{R\in O^{3\times q}}\left\|vec\left(\hat{R}_z - R\right)\right\|_{Q_{\hat{R}}}\right)}_{F(Z)} \end{aligned} \tag{19}$$

In this minimization problem, we first estimate the attitude matrix $\hat{R}_Z$, which is conditioned on the estimation of the ambiguities, as follows:

$$\begin{aligned} vec\left(\hat{R}_Z\right) &= vec\left(\hat{R}\right) - Q_{\hat{R}\hat{Z}}Q_{\hat{Z}}^{-1}vec\left(\hat{Z}-Z\right) \\ Q_{\hat{R}_Z} &= Q_{\hat{R}} - Q_{\hat{R}\hat{Z}}Q_{\hat{Z}}^{-1}Q_{\hat{Z}\hat{R}} \end{aligned} \tag{20}$$

Equation (19) shows that the estimation of the fixed ambiguity solution involves minimizing the objective function $F(Z)$ while conditioning the attitude matrix estimation $vec\left(\hat{R}_Z\right)$. This inclusion of a nonlinear constraint in the A-PAD model makes the search space for the integer ambiguities non-ellipsoidal and complex. To address this challenge, constrained searching methods such as search-and-expand and search-and-shrink algorithms are defined to bound the minimization objective function and the designated searching space (Giorgi et al., 2008; Giorgi, 2017). For instance, in the search-and-expand method, a lower bound is defined for the minimization objective function, and a search space for that lower bound is considered. The integer search is performed: if any candidates are found, the minimization objective function is evaluated for the candidates, and the candidate that returns the smallest value is the integer minimizer. If there are no candidates in this search space, the lower bound is expanded in another round. The fixed attitude matrix is estimated by substituting the integer ambiguities in Equation (20) with $vec\left(\hat{R}_{\check{Z}}\right)$, which leads to a mixed ambiguity–attitude minimization problem.

Because of the complexity of the search space in the multi-constrained A-PAD model for populated arrays with more than three antennae, a set of linear constraints was implemented, leading to the application of the affine-constrained concept (Teunissen, 2012a), which can be modeled as follows:

$$E\left(vec\left(Y\right)\right) = AZ + GB, \quad BS = 0 \tag{21}$$

This affine definition comes from the orthonormal matrix parametrization, which allows us to use the basis matrix (S) of the null space of B and update our A-PAD model with the equivalent implicit form of $B = RB_0$ as $BS = 0$. By doing this, we ignore the quadratic constraints and consider only the linear constraints. This replacement ensures a high probability of success for integer ambiguity resolution. The procedure of the affine-constrained A-PAD model is similar to that of the multi-constrained model. However, by defining the projector $P_S = S(S^T PS)^{-1} S^T P$, we can write the ambiguity objective function for the affine-constrained model as follows:

$$F_A\left(Z\right) = \left\| vec\left(\hat{Z} - Z\right)\right\|_{Q_{\hat{Z}}} + \min_{R \in O^{3\times q}} \left\| vec\left(\hat{B}\left(Z\right)P_S\right)\right\|_{Q_{\hat{B}(Z)}} \tag{22}$$

In contrast to the objective function in Equation (19), the above objective function provides an ellipsoidal search space with lower complexity and less computational burden. Thus, the affine-constrained A-PAD model is more efficient for CubeSats with limited power and processing resources.

To apply this approach in real-time mode and make it suitable for onboard processing, A-POD and A-PAD modules were implemented in the LeoPod software (Allahvirdizadeh, 2022). Figure 2 presents a flow diagram summarizing the proposed module for the ADCS based on our models. The observations obtained from the array are utilized to estimate the attitude angles and integer ambiguities within the A-PAD module. This estimation process can be conducted using either a multi-constrained or affine-constrained approach. Subsequently, these observations are decorrelated to improve their accuracy, and then, the fixed integer ambiguities are taken into account to reconstruct the A-POD observations. Finally, the POD procedure can be initiated, utilizing the reconstructed A-POD observations. During this process, the estimated attitude angles are employed as required, facilitating an accurate determination of the CubeSat's precise orbit. Data quality control

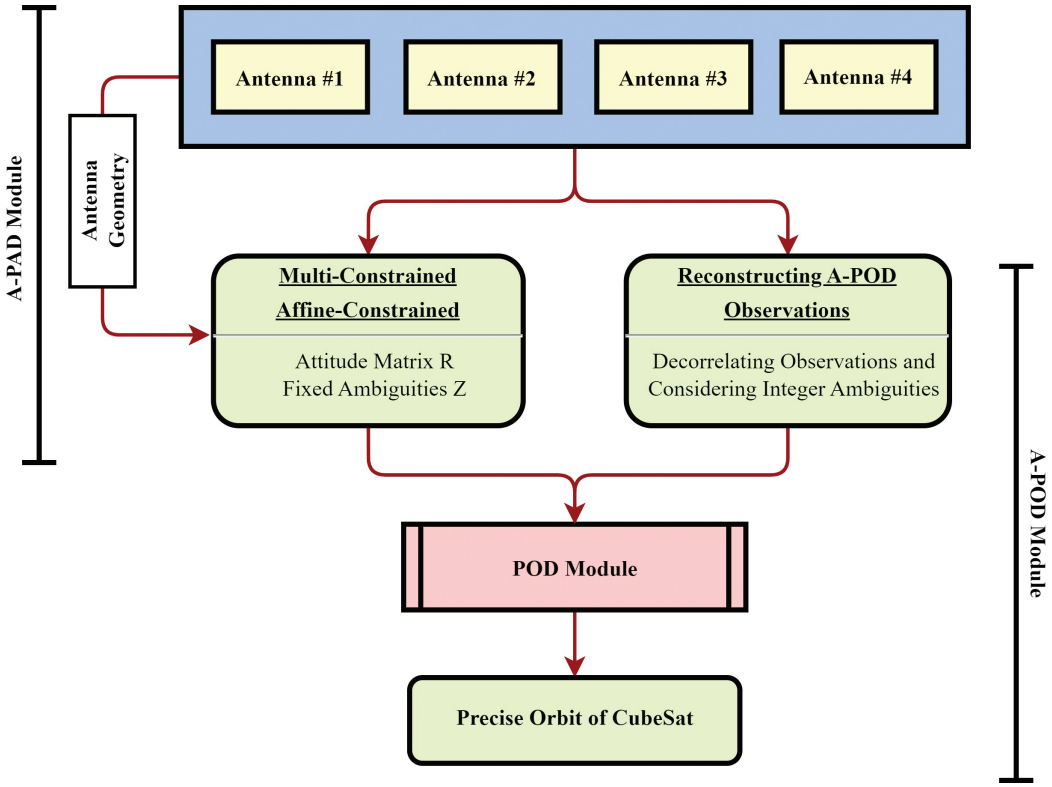

FIGURE 2 Flow diagram of A-POD and A-PAD modules implemented in the LeoPod software

is performed by applying statistical testing using the detection, identification, and adaptation method inside the filter (Teunissen, 2006).

By integrating the A-PAD and A-POD modules, our approach leverages the benefits of both precise attitude and precise orbit determination, resulting in improved accuracy and performance. To validate the A-POD and A-PAD algorithms, an antenna array is required. However, to our knowledge, no CubeSat is currently equipped with more than one GNSS antenna. Therefore, a simulated antenna array for a CubeSat using actual onboard observations is used in our tests to demonstrate the proposed method.

3 | TESTING

3.1 | Test Description

In this section, we present a simulation of an antenna array, illustrated in Figure 3. The size of the array and the proximity of the antennae within it are critical design factors, primarily dictated by the constraints of the CubeSat structure. The close proximity of the antennae (less than half of the signal wavelength) introduces mutual coupling and pattern distortion effects, which can impact signal correlation and the effectiveness of conventional signal processing and models designed for independent or uncorrelated signals. Meanwhile, pattern distortion can potentially cause frequency shifts that compromise proper functionality within the designated frequency band. To mitigate such effects, it is crucial to consider an appropriate distance between the antennae during the array design phase.

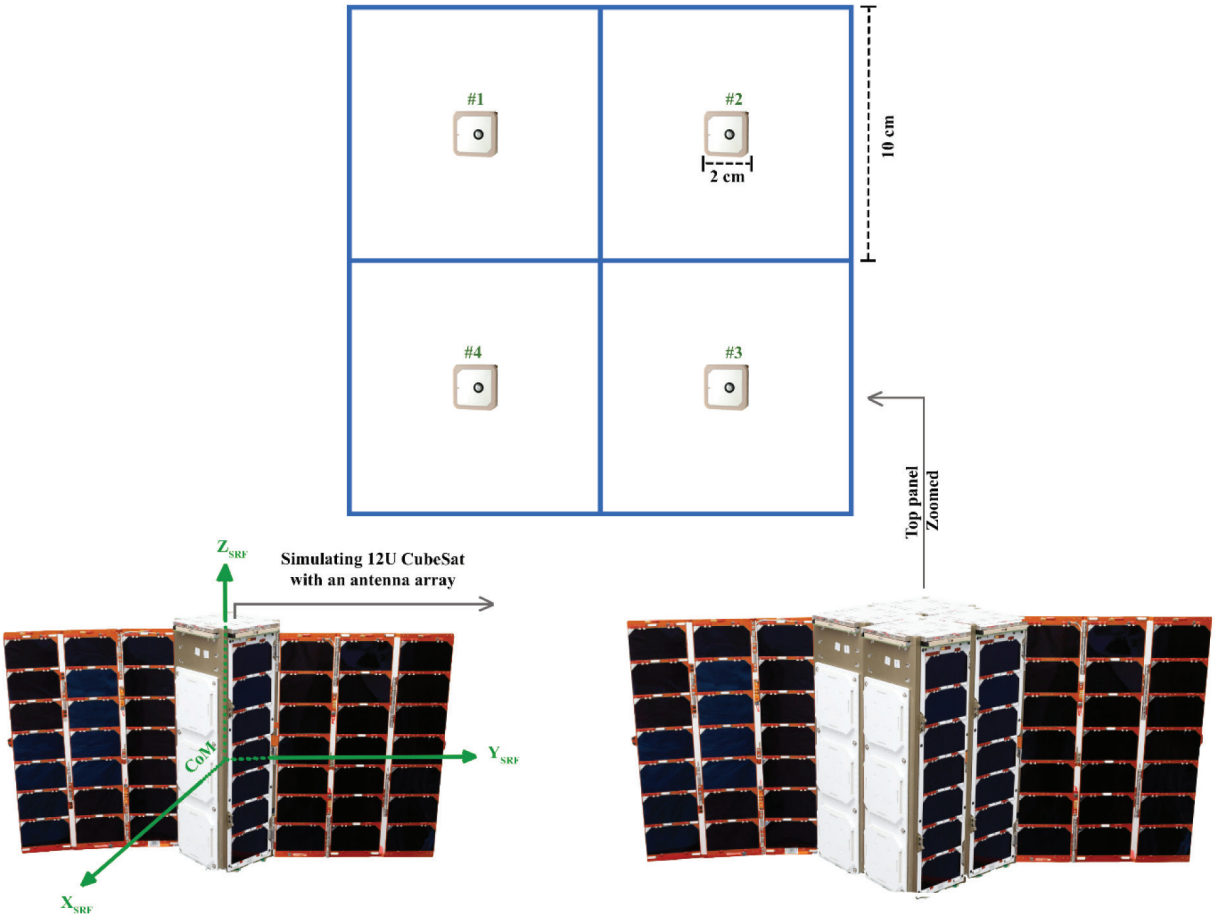

FIGURE 3 Layout of the simulated antenna array

The optimal distance between antenna elements in an array is more than half the wavelength of the designated frequencies, which, for our case in which GPS L1 is the higher frequency used, is roughly 10 cm.

The left CubeSat depicted in Figure 3 is a three-unit (3U) Spire CubeSat that we selected for the testing. The size of the top panel is 10×10 cm^2, where placing the array on this panel would not be feasible because of the mutual coupling and pattern distortions it would introduce. Alternatives such as placing antennae on the side panels could be explored to avoid these effects; however, this approach presents challenges regarding the number of satellites tracked by the receiver, which requires further investigation. Additionally, there are template constraints for each satellite based on its mission and the capacity of the bus and payloads, which are beyond the scope of this paper.

To address these considerations, we assumed that the 3U CubeSat is expanded to a 12U CubeSat and simulated an array of four antennae on the top panel of this CubeSat, as depicted in Figure 3. Antenna #1 serves as the main POD antenna, whereas the remaining antennae are simulated based on their coordinates in the SRF, as explained in the next section.

It is worth mentioning that the near-field environment, including other available sensors, may further amplify the aforementioned effects. In addition to constraints on the size of the array and the distances between antennae, this complexity necessitates pre-flight tests and in-flight calibration of both absolute and relative antenna phase patterns (Montenbruck, 2017).

TABLE 2
Coordinates of the Center of the Simulated Antennae in the SRF

Antenna	#1	#2	#3	#4
Coordinates (cm)	[0, 0, –16.31]	[0, 10, –16.31]	[–10, 10, –16.31]	[–10, 0, –16.31]

TABLE 3
CubeSat Specifications Employed in This Study

ID	Name	COSPAR ID	Altitude	Orbit Type
099	LEMUR-2-JOHANLORAN	2019-018G	505 km	Sun-synchronous orbit (local time of descending node 09:30)

Table 2 provides the coordinates of the simulated antennae in the SRF. The SRF's orientation for the Spire CubeSats is defined as follows (personal communication with the Spire team):

- The Z-axis points towards the zenith direction.
- The Y-axis points towards the negative orbit normal.
- The X-axis is approximately aligned with the velocity direction but orthogonal to the Y-axis.

These axes are joined at the center of mass (CoM) of the CubeSat, as shown in Figure 3.

3.2 | Observation Simulation

To generate observations for the simulated antennae connected to one receiver, we utilized actual GNSS observations acquired by the main POD antenna. The observations correspond to data collected on 1 January 2022 for the CubeSat with the specifications given in Table 3. These observations were processed using reduced-dynamic POD, employing the specifications outlined in Table 4. The processing was performed using Bernese processing software v5.4 (Dach et al., 2015).

The CubeSat's POD procedure and output orbit have been evaluated by Allahvirdi-Zadeh, Wang, & El-Mowafy (2022) through various validation methods. The reduced-dynamic orbit, denoted as $r_{0,POD}$, and the attitude matrix from the onboard ADCS of the CubeSats $\left(R_0\right)$ are used to generate a user motion format (.umt) to feed the SimGEN simulation software, assumed as the true trajectory of the CubeSat (Spirent, 2022). The precise coordinates of GNSS satellites in the ECEF frame $\left(r^s_{IGS}\right)$, as well as clock corrections $\left(dt^s_{IGS}\right)$ of these satellites in ranges, are utilized from final products from the International GNSS Service (Johnston et al., 2017). To account for ionospheric delays $\left(i^s_{r,f}\right)$ for each frequency, the following spacecraft ionospheric model implemented in SimGEN is employed:

$$i^s_{r,f} = \frac{82.1 \times TEC}{f^2 \times \left(\sqrt{\sin^2 e + 0.076} + \sin e\right)} \tag{23}$$

where TEC is the total electron content and e denotes the elevation angle of the GNSS satellite. This simulation includes noise levels similar to those considered for the reduced-dynamic POD for the raw observations, given in Table 4. These combined noises and multipath errors are denoted as ε_p and ε_φ for code and phase

TABLE 4
POD Processing Models and Parameters

Item	Description
Dynamic models and Stochastic accelerations	Gravity field: Earth Gravitational Model (EGM 2008) (Pavlis et al., 2008)
	Tidal corrections: FES2014b (Lyard et al., 2021)
	Relativity: International Earth Rotation and Reference Systems Service (IERS 2010) (Petit & Luzum, 2010)
	Planet ephemeris: Jet Propulsion Laboratory (JPL DE421) (Standish, 1998)
	Velocity changes (pulses) and piecewise constant accelerations
Observation model	Observation model: Ionospheric-free linear combination of 1-Hz GPS code (C1, C2) and phase (L1, L2); Stochastic model: SNR-based weighting model (Allahvirdi-Zadeh, El-Mowafy, & Wang, 2022)
	Eclipsed observations: Removed using the shadow model (Allahverdi-Zadeh et al., 2016)
	Code and phase standard deviation: 0.1 m and 1 mm (Zenith, L1)
	Satellite attitude information: Obtained as quaternions
	Antenna phase center offset: [0.0021, 0.0011, –0.0223] m for L1 [0.0033, 0.0034, –0.0125] m for L2 Antenna phase center variation pattern: Residual approach (Allahvirdi-Zadeh, 2021)
	Phase ambiguities: Fixed by applying observable-specific signal biases (Schaer et al., 2021)

observations, respectively. Because the A-POAD model is based on forming differenced observations, the receiver clock offsets are ignored in the simulation. These specifications enable us to simulate 1-Hz observations for the designed antenna array as follows:

$$\begin{aligned} p^s_{r,f} &= \left\| \left(r_{0,POD} + TR_0 r_i \right) - r^s_{IGS} \right\| - dt^s_{IGS} + i^s_{r,f} + \varepsilon_p \\ \varphi^s_{r,f} &= \left\| \left(r_{0,POD} + TR_0 r_i \right) - r^s_{IGS} \right\| - dt^s_{IGS} - i^s_{r,f} + \lambda_f n^s_r + \varepsilon_\varphi \end{aligned} \tag{24}$$

where r_i indicates the SRF coordinates of each antenna provided in Table 2, transformed from the inertial frame into the ECEF frame via the T matrix. In this study, we focused solely on GPS observations, as there are currently no data for a CubeSat equipped with a multi-GNSS receiver. However, future investigations will include multi-GNSS data.

To assess the accuracy and effectiveness of our developed method, we designed and conducted several tests. A comprehensive discussion of these validation tests will be presented in the next section.

3.3 | Testing Approach

To validate the A-POD and A-PAD models, we begin by testing the developed attitude model using single- and dual-frequency GPS observations. This test showcases the model's suitability for CubeSats, regardless of the receiver type with which they are equipped. To assess the complexity of the array geometry, we evaluate both multi-constrained and affine-constrained models, considering arrays of

3 or 4 antennae. Next, we use the A-POD observations in a POD module to evaluate the A-POD model and illustrate the applicability of our model for CubeSats.

3.4 | Testing Results

In the initial test, we utilize simulated GPS observations obtained from an antenna array to estimate attitude angles. The estimation is performed twice, first with dual-frequency and then with single-frequency observations. The latter is important for CubeSats, as they often face power constraints that may restrict them to single-frequency observations. The primary objective of this test is to examine the effects of this constraint on data collection and its impact on the overall analysis.

Figure 4 illustrates the roll and pitch angles while ambiguities are resolved as float and fixed values via the A-PAD model for 24 h of 1-Hz GPS observations. These solutions are called "float" and "fixed" attitude angles, respectively. The left and right columns of the figure depict the dual-frequency and single-frequency cases, respectively. It is evident from the figure that ambiguity resolution has a notable impact on the estimated roll and pitch angles. Utilizing the antenna array in the A-PAD model not only enhances the precision of the estimated rotation angles but

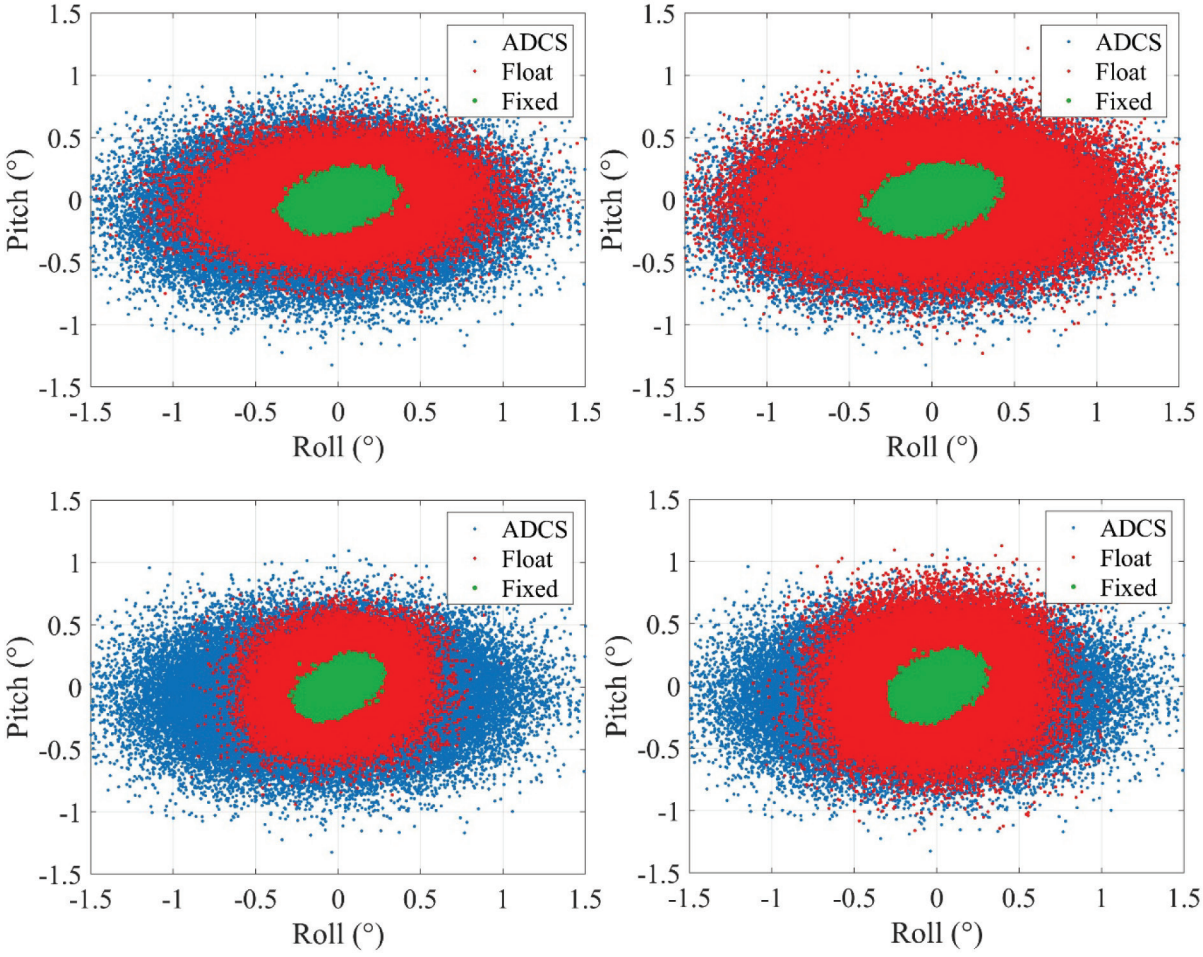

FIGURE 4 Roll and pitch attitude angles estimated from dual-frequency (left column) and single-frequency (right column) observations for MC A-PAD (top row) and AC A-PAD (bottom row)

also renders the estimations more precise compared with magnetometers and sun sensors. The Spire CubeSat is equipped with a combination of these sensors in the ADCS (Spire, 2023), and their outputs are shown in the figure to visually confirm the accuracy of the A-PAD model with the antenna array. Additionally, this array configuration is more cost-effective, further emphasizing its advantage over alternative sensor options (see Table 1). Figure 4 consists of two rows, where the top row corresponds to the application of the multi-constrained (MC A-PAD) model, and the bottom row represents the affine-constrained (AC A-PAD) model. In the MC A-PAD case, the array utilizes antennae 1, 2, and 3, whereas the AC A-PAD model employs the entire array. The inclusion of an additional antenna and the consideration of the relevant constraint in the AC A-PAD model result in improved attitude angle estimates, regardless of whether single- or dual-frequency observations are used. This enhancement is the primary advantage of the AC A-PAD attitude model.

Given that the antennae are positioned on the top panel perpendicular to the Z-axis of the SRF, fixing ambiguities is not expected to have a substantial impact on the estimated yaw angle unless the CubeSat undergoes rotation around its Z-axis. This specific scenario is illustrated in Figure 5 for one of the testing cases, i.e., MC A-PAD with dual-frequency observations. The outcomes of the other tests exhibit similar patterns, further supporting the notion that fixing ambiguities primarily affects the roll and pitch angles. This result arises because the baselines rotate around the Z-axis simultaneously. Exploring alternative antenna configurations, such as configurations in which one antenna is placed on the side panels or bottom of the CubeSat, may help ascertain the impact of fixed ambiguity on the yaw angle. Such exploration is limited by the structural constraints of CubeSats and the potential for signal blockage from GNSS satellites and will be considered in a future study.

As mentioned earlier, the attitude angles in this CubeSat are a combination of magnetometer and sun sensor outputs. However, the low precision of these kinds of sensors, as indicated in Table 1 and evident from Figures 4 and 5, prevents them from being considered the best reference, in contrast to star trackers. Considering this limitation, we will apply the estimated attitude angles from the A-PAD model in the final POD test. A successful POD output implicitly validates the accuracy of the estimated attitude angles.

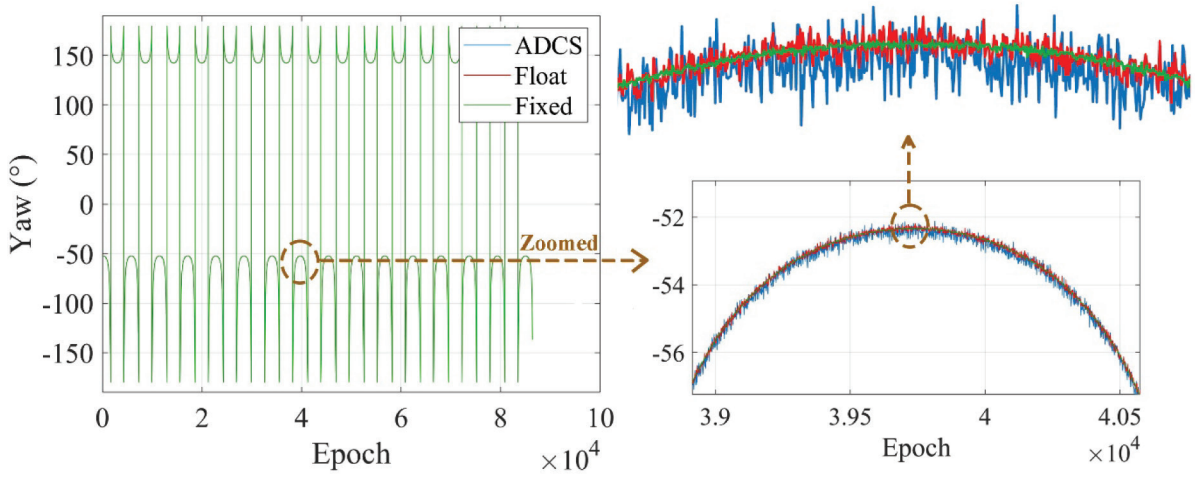

FIGURE 5 Yaw attitude angle, with magnified results shown for a duration of approximately 20 min on the right

TABLE 5
RMS Values of the Differences Between Estimated Orbits and the Reference Orbit

Observations	X (m)	Y (m)	Z (m)	3D
One antenna	0.069	0.051	0.081	0.118
A-POD with FOUR antennae	0.022	0.016	0.031	0.041

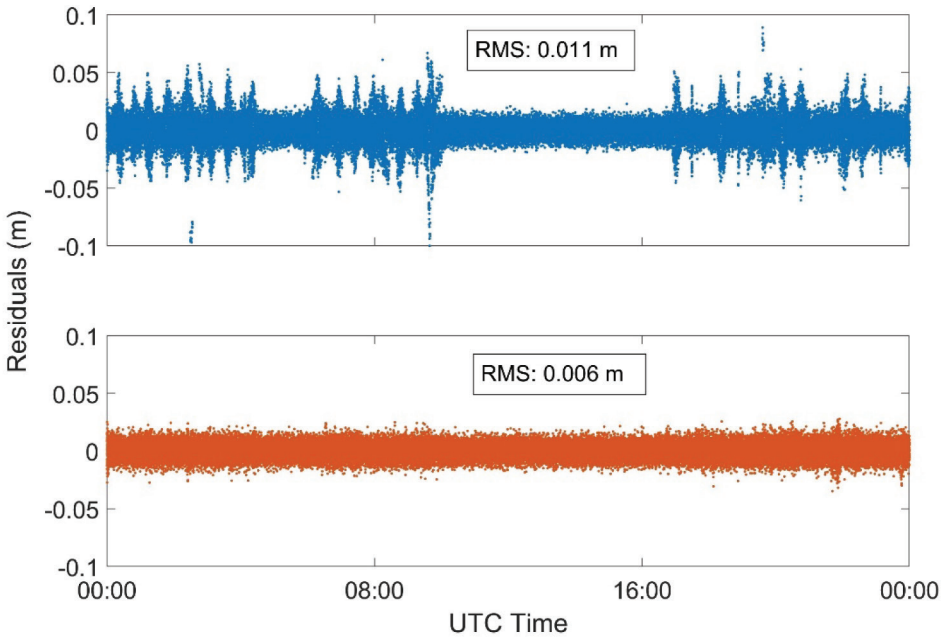

FIGURE 6 Observation residuals from conventional POD with one antenna (top) and A-POD with a full array (bottom); UTC: coordinated universal time

The final step involves evaluating the A-POD model. The reconstructed observations from Equation (16) are processed in a kinematic POD, as illustrated in Figure 2. A comparison between these orbits and the reference reduced-dynamic orbit from the Bernese software verifies that our A-POD model significantly enhances the accuracy of all orbital components (3D root mean square [RMS] = 4.1 cm), surpassing the results obtained when utilizing a single antenna (3D RMS = 11.8 cm) with quaternions. Table 5 provides a summary of the RMS values for the discrepancies between the orbit from the A-POD model and the reference orbit. It is important to highlight that this test also serves as an evaluation of the impact of the attitude matrix used in the estimated orbits. This evaluation involves applying the transformation in various parts of the POD process, including the consideration of antenna sensor offsets. By conducting this evaluation, we can gain insights into the performance and accuracy of the attitude matrix in POD. Future investigations will also explore the application of the attitude matrix in a wider range of operational situations, such as pointing operations and formation flying maneuvers.

The final stage of evaluation involves conducting an observation residual analysis. As depicted in Figure 6, the residuals of all observations in the A-POD model show significantly smoother behavior compared with conventional POD with a single antenna. The RMS value of the residuals for the A-POD model is 6 mm, which is approximately half the value obtained from conventional POD using one antenna. This substantial RMS reduction confirms the superior performance and

optimality of the proposed A-POD model in comparison to typical POD processing. Importantly, the outcomes of the A-POD model remain consistent, regardless of whether an MC or AC A-PAD approach is utilized in deriving the observations outlined in Equation (16).

It is worth noting that the performance of the developed model will be affected if frequent signal interruptions and initializations occur, as the A-POAD concept relies on the kinematic POD approach, where disruptions in the collection of GNSS data have the potential to trigger a recalculation reset. Naturally, the GNSS observation noise and quality will affect any positioning method.

4 | CONCLUSION

CubeSats offer promising prospects for various applications. However, their consideration for LEO-PNT systems necessitates higher orbital accuracy and reliable attitude determination. Current COTS sensors may not be suitable for achieving these requirements because of the low-cost requirements of CubeSat missions.

In this study, we have developed a combined A-POAD model specifically designed for CubeSats. The correlation between observations within the combined model is addressed through the use of DD observations and the estimation of fixed ambiguities of the array, facilitated by the A-PAD model. The estimation process can be conducted using the developed multi-constrained or affine-constrained models. The performance of these models has been evaluated through both single- and dual-frequency observations.

The accuracy of the solution with determined integer ambiguities in the A-PAD model has been confirmed visually and in the POD validation. This finding highlights the advantage of the A-PAD model for CubeSats, as employing an array for attitude determination is significantly more cost-effective than using expensive, precise star trackers while still providing accurate attitude angles.

The results presented herein demonstrate that the A-POD observations offer improved accuracy compared with original observations. The orbital components derived from the POD process using these observations show enhanced accuracy compared with the use of original observations alone. Furthermore, the estimated observation residuals display a smoother pattern, and the RMS is reduced by a factor of almost 2 compared with that obtained from observations using only one antenna. These findings confirm the efficiency and effectiveness of the A-POD model and implicitly validate the output of the A-PAD model.

The estimated attitude and orbit based on the developed A-PAD and A-POD concepts hold potential for CubeSats in missions that demand highly precise orbit and attitude determination, such as LEO-PNT systems. The developed method is also applicable to formation flying scenarios, wherein a collection of small satellites operate in proximity. In such scenarios, determining the attitude and orbit of the entire platform is essential.

ACKNOWLEDGMENTS

The authors would like to express their gratitude to Spirent for providing access to the SimGEN software, which helped in simulating and evaluating various scenarios throughout this research. Additionally, the authors would like to acknowledge the contributions of the previous members of the GNSS Research Center in developing the MC-LAMBDA software. Funding of this research work by the Australian Research Council under the Discovery Project (DP240101710) is acknowledged.

REFERENCES

Allahvirdi-Zadeh, A. (2021). Phase centre variation of the GNSS antenna onboard the cubesats and its impact on precise orbit determination. *Proc. of the GSA Earth Sciences Student Symposium, Western Australia (GESSS-WA)*, Perth, Western Australia. https://doi.org/10.13140/RG.2.2.10355.45607/1

Allahverdi-Zadeh, A., Asgari, J., & Amiri-Simkooei, A. R. (2016). Investigation of GPS draconitic year effect on GPS time series of eliminated eclipsing GPS satellite data. *Journal of Geodetic Science*, *6*(1), 93–102. https://doi.org/10.1515/jogs-2016-0007

Allahvirdi-Zadeh, A., Awange, J., El-Mowafy, A., Ding, T., & Wang, K. (2022). Stability of cubesat clocks and their impacts on GNSS radio occultation. *Remote Sensing*, *14*(2), 1–26. https://doi.org/10.3390/rs14020362

Allahvirdi-Zadeh, A., & El-Mowafy, A. (2021). Precise orbit determination of cubesats using a proposed observations weighting model. *Proc. of the Scientific Assembly of the International Association of Geodesy (IAG),* Beijing, China, 387–384. https://doi.org/10.13140/RG.2.2.20619.62244/1

Allahvirdi-Zadeh, A., & El-Mowafy, A. (2022a). CubeSat's attitude determination using GNSS antenna array. *Proc. of the International Global Navigation Satellite Systems Conference 2022 (IGNSS)*, UNSW, Sydney. https://doi.org/10.13140/RG.2.2.29925.68320

Allahvirdi-Zadeh, A., & El-Mowafy, A. (2022b). The impact of precise inter-satellite ranges on relative precise orbit determination in a smart cubesats constellation. *Proc. of the EGU General Assembly Conference Abstracts*, Vienna, Austria, EGU22–2215. https://doi.org/10.5194/egusphere-egu22-2215

Allahvirdi-Zadeh, A., El-Mowafy, A., Mcclusky, S., Allgeyer, S., & Hammond, A. (2024). Ginan supporting future LEO-PNT. *Proc. of the Proc. of the International Global Navigation Satellite Systems Conference 2024 (IGNSS)*, Sydney, NSW. https://doi.org/10.13140/RG.2.2.22771.30248

Allahvirdi-Zadeh, A., El-Mowafy, A., & Wang, K. (2022). Precise orbit determination of cubesats using proposed observations weighting model. In Freymueller, J.T., Sánchez, L. (Eds.), *Geodesy for a sustainable earth. International Association of Geodesy Symposia* (vol. 154, 377–384). Springer, Cham. https://doi.org/10.1007/1345_2022_160

Allahvirdi-Zadeh, A., El-Mowafy, A., & Wang, K. (2024). Leveraging future LEO constellations for the precise orbit determination of lower small satellites. *Proc. of the 2024 International Technical Meeting of the Institute of Navigation,* Long Beach, CA, 756–769. https://doi.org/10.33012/2024.19485

Allahvirdi-Zadeh, A., Wang, K., & El-Mowafy, A. (2021). POD of small LEO satellites based on precise real-time MADOCA and SBAS-aided PPP corrections. *GPS Solutions*, *25*(31), 1–14. https://doi.org/10.1007/s10291-020-01078-8

Allahvirdi-Zadeh, A., Wang, K., & El-Mowafy, A. (2022). Precise orbit determination of LEO satellites based on undifferenced GNSS observations. *Journal of Surveying Engineering*, *148*(1), 03121001. https://doi.org/10.1061/(ASCE)SU.1943-5428.0000382

Allahvirdizadeh, A. (2022). *Precise orbit determination of cubesats* [Doctoral thesis, Curtin University]. Curtin Theses. http://hdl.handle.net/20.500.11937/89922

Arnold, D., Peter, H., Mao, X., Miller, A., & Jäggi, A. (2023). Precise orbit determination of Spire nano satellites. *Advances in Space Research, 72*(11), 5030–5046. https://doi.org/10.1016/j.asr.2023.10.012

Cohen, C. E., Lightsey, E. G., Parkinson, B. W., & Feess, W. A. (1994). Space flight tests of attitude determination using GPS. *International Journal of Satellite Communications*, *12*(5), 427–433. https://doi.org/10.1002/sat.4600120504

Cohen, C. E., Parkinson, B. W., & McNally, B. D. (1994). Flight tests of attitude determination using GPS compared against an inertial navigation unit. *NAVIGATION*, *41*(1), 83–97. https://doi.org/10.1002/j.2161-4296.1994.tb02323.x

Dach, R., Lutz, S., Walser, P., & Fridez, P. (2015). *Bernese GNSS software version 5.2*. Bern Open Publishing. https://doi.org/10.7892/boris.72297

El-Mowafy, A., Wang, K., & Allahverdi-Zadeh, A. (2022). The potential of LEO mega-constellations in aiding GNSS to enable positioning in challenging environments. *Proc. of the XXVII International Federation of Surveyors (FIG) Congress,* Warsaw, Poland, 1–11. https://api.semanticscholar.org/CorpusID:264148693

Freesland, D., Reiss, K., Young, D., Cooper, J., & Adams, C. A. (1996). GPS based attitude determination: The REX II flight experience. https://digitalcommons.usu.edu/smallsat/1996/all1996/5/

Giorgi, G. (2017). Attitude determination. In P. J. G. Teunissen & O. Montenbruck (Eds.), *Springer handbook of global navigation satellite systems*, 781–809. Springer International Publishing. https://doi.org/10.1007/978-3-319-42928-1_27

Giorgi, G., Teunissen, P., & Buist, P. (2008). A search and shrink approach for the baseline constrained LAMBDA method: Experimental results. *Proc. of the International GPS/GNSS Symposium,* Tokyo, Japan. http://gnss.curtin.edu.au/wp-content/uploads/sites/21/2016/04/Giorgi2008search.pdf

Giorgi, G., Teunissen, P. J. G., & Gourlay, T. P. (2012). Instantaneous global navigation satellite system (GNSS)-based attitude determination for maritime applications. *IEEE Journal of Oceanic Engineering*, *37*(3), 348–362. https://doi.org/10.1109/JOE.2012.2191996

Giorgi, G., Teunissen, P. J. G., Verhagen, S., & Buist, P. J. (2012). Instantaneous ambiguity resolution in global-navigation-satellite-system-based attitude determination applications: A multivariate constrained approach. *Journal of Guidance, Control, and Dynamics*, *35*(1), 51–67. https://doi.org/10.2514/1.54069

Giorgi, G., Verhagen, S., Buist, P. J., & Teunissen, P. J. G. (2011). GNSS-based attitude determination aerospace and formation flying. *Inside GNSS*, *6*(4), 62–71. https://gnss.curtin.edu.au/wp-content/uploads/sites/21/2016/04/Giorgi2011GNSS-based.pdf

Gomez, S. (2005). *Three years of Global Positioning System experience on International Space Station* (NASA/TM-2005-213715). https://ntrs.nasa.gov/citations/20070018309

Hauschild, A., & Montenbruck, O. (2021). Precise real-time navigation of LEO satellites using GNSS broadcast ephemerides. *NAVIGATION, 68*(2), 419–432. https://doi.org/10.1002/navi.416

Hauschild, A., Montenbruck, O., & Langley, R. B. (2020). Flight results of GPS-based attitude determination for the Canadian CASSIOPE satellite. *NAVIGATION*, *67*(1), 83–91. https://doi.org/10.1002/navi.348

Jiang, M., Qin, H., Zhao, C., & Sun, G. (2021). LEO Doppler-aided GNSS position estimation. *GPS Solutions, 26*(1), 31. https://doi.org/10.1007/s10291-021-01210-2

Jin, B., Chen, S., Li, M., Yue, F., & Zhao, L. (2022). Sentinel-6A attitude modeling with dual GNSS antennas and its impact on precise orbit determination. *GPS Solutions*, *27*(7), 1–13. https://doi.org/10.1007/s10291-022-01346-9

Johnston, G., Riddell, A., & Hausler, G. (2017). The International GNSS Service. *Springer handbook of global navigation satellite systems*. https://doi.org/10.1007/978-3-319-42928-1_33

Li, B., & Teunissen, P. J. G. (2014). GNSS antenna array-aided CORS ambiguity resolution. *Journal of Geodesy*, *88*(4), 363–376. https://doi.org/10.1007/s00190-013-0688-2

Li, X., Ma, F., Li, X., Lv, H., Bian, L., Jiang, Z., & Zhang, X. (2019). LEO constellation-augmented multi-GNSS for rapid PPP convergence. *Journal of Geodesy, 93*(5), 749–764. https://doi.org/10.1007/s00190-018-1195-2

Lyard, F. H., Allain, D. J., Cancet, M., Carrère, L., & Picot, N. (2021). FES2014 global ocean tide atlas: Design and performance. *Ocean Science, 17*(3), 615–649. https://doi.org/10.5194/os-17-615-2021

Montenbruck, O. (2017). Space applications. In P. J. G. Teunissen & O. Montenbruck (Eds.), *Handbook of global navigation satellite systems*, 933–964. Springer. https://doi.org/10.1007/978-3-319-42928-1_32

Nadarajah, N., & Teunissen, P. J. G. (2014). Instantaneous GPS/Galileo/QZSS/SBAS attitude determination: A single-frequency (L1/E1) robustness analysis under constrained environments. *NAVIGATION*, *61*(1), 65–75. https://doi.org/10.1002/navi.51

Nadarajah, N., Teunissen, P., & de Bakker, P. (2014). GNSS array-aided positioning and attitude determination: Real data analyses. *Proc. of the 27th International Technical Meeting of the Satellite Division of the Institute of Navigation (ION GNSS+ 2014),* Tampa, FL, 2544–2554. https://www.ion.org/publications/abstract.cfm?articleID=12447

Nadarajah, N., Teunissen, P. J. G., Buist, P. J., & Steigenberger, P. (2012). First results of instantaneous GPS/Galileo/COMPASS attitude determination. *Proc. of the 2012 6th ESA Workshop on Satellite Navigation Technologies (Navitec 2012) & European Workshop on GNSS Signals and Signal Processing,* Noordwijk, Netherlands, 1–8. https://doi.org/10.1109/NAVITEC.2012.6423068

Nadarajah, N., Teunissen, P. J. G., & Raziq, N. (2013). Instantaneous GPS–Galileo attitude determination: Single-frequency performance in satellite-deprived environments. *IEEE Transactions on Vehicular Technology*, *62*(7), 2963–2976. https://doi.org/10.1109/TVT.2013.2256153

Nadarajah, N., Teunissen, P. J. G., & Verhagen, S. (2016). Attitude determination and relative positioning for LEO satellites using arrays of GNSS sensors. In C. Rizos &, P. Willis (Eds.) *IAG 150 Years*. Springer, Cham. https://doi.org/10.1007/1345_2015_26

Palomo, J. M., D'Angelo, P., Silva, P. F., Fernández, A. J., Giordano, P., Zoccarato, P., Tegedor, J., Oerpen, O., Hansen, L. B., Hill, C., & Moore, T. (2019). Space GNSS receiver performance results with precise real-time on-board orbit determination (P2OD) in LEO missions. *Proc. of the 32nd International Technical Meeting of the Satellite Division of the Institute of Navigation (ION GNSS+ 2019),* Miami, FL, 1172–1186. https://doi.org/10.33012/2019.17082

Pavlis, N., Kenyon, S., Factor, J., & Holmes, S. (2008). Earth gravitational model 2008. In *SEG Technical Program Expanded Abstracts 2008* (pp. 761–763). Society of Exploration Geophysicists. https://doi.org/10.1190/1.3063757

Petit, G., & Luzum, B. (2010). In G. Petit & B. Luzum (Eds.) *International Earth Rotation and Reference Ststems Service (IERS) Conventions 2010,* 179. https://www.iers.org/IERS/EN/Publications/TechnicalNotes/tn36.html

Schaer, S., Villiger, A., Arnold, D., Dach, R., Prange, L., & Jäggi, A. (2021). The CODE ambiguity-fixed clock and phase bias analysis products: Generation, properties, and performance. *Journal of Geodesy*, *95*(7), 81 (1–25). https://doi.org/10.1007/s00190-021-01521-9

Schott, J. R. (2016). *Matrix analysis for statistics*. John Wiley & Sons. https://www.wiley.com/en-br/Matrix+Analysis+for+Statistics%2C+3rd+Edition-p-9781119092469

Spire. (2023). Attitude determination and control system (ADCS). https://spire.com/spirepedia/attitude-determination-and-control-system-adcs/

Spirent. (2022). *SimGEN® software user manual for version v8.01.00. Software for the Spirent range of satellite navigation simulator products*. Spirent Communications, PLC. https://www.spirent.com/assets/u/datasheet-simgen

Standish, E. (1998). JPL planetary and lunar ephemerides, DE405/LE405. *JPL IOM, 312, F-98_048*. https://ssd.jpl.nasa.gov/planets/eph_export.html

Teunissen, P. J. G. (2006). *Testing theory; an introduction* (2nd ed.). Series on Mathematical Geodesy and Positioning. VSSD. https://research.tudelft.nl/en/publications/testing-theory-an-introduction-2nd-edition

Teunissen, P. (2007). The LAMBDA method for the GNSS compass. *Artificial Satellites*, *41*(3), 89–103. https://doi.org/doi:10.2478/v10018-007-0009-1

Teunissen, P. (2008). A general multivariate formulation of the multi-antenna GNSS attitude determination problem. *Artificial Satellites*, *42*(2), 97–111. https://doi.org/doi:10.2478/v10018-008-0002-3

Teunissen, P. J. G. (2010). Integer least-squares theory for the GNSS compass. *Journal of Geodesy*, *84*(7), 433–447. https://doi.org/10.1007/s00190-010-0380-8

Teunissen, P. J. G. (2012a). The affine constrained GNSS attitude model and its multivariate integer least-squares solution. *Journal of Geodesy*, *86*(7), 547–563. https://doi.org/10.1007/s00190-011-0538-z

Teunissen, P. J. G. (2012b). A-PPP: Array-aided precise point positioning with global navigation satellite systems. *IEEE Transactions on Signal Processing*, *60*(6), 2870–2881. https://doi.org/10.1109/TSP.2012.2189854

Unwin, M., Purivigraipong, P., da Silva Curiel, A., & Sweeting, M. (2002). Stand-alone spacecraft attitude determination using real flight GPS data from UOSAT-12. *Acta Astronautica*, *51*(1), 261–268. https://doi.org/10.1016/S0094-5765(02)00038-3

Wang, K., Allahvirdi-Zadeh, A., El-Mowafy, A., & Gross, J. N. (2020). A sensitivity study of POD using dual-frequency GPS for cubesats data limitation and resources. *Remote Sensing*, *12*(13), 2107. https://doi.org/10.3390/rs12132107

Wu, S., Zhao, X., Pang, C., Zhang, L., Xu, Z., & Zou, K. (2020). Improving ambiguity resolution success rate in the joint solution of GNSS-based attitude determination and relative positioning with multivariate constraints. *GPS Solutions*, *24*(1), 31 (1–14). https://doi.org/10.1007/s10291-019-0943-y

How to cite this article: Allahvirdi-Zadeh, A., & El-Mowafy, A. (2024). Array-aided precise orbit and attitude determination of CubeSats using GNSS. *NAVIGATION, 71*(3). https://doi.org/10.33012/navi.651

APPENDIX

For an array of a antennae connecting to one receiver, where each antenna collects code and phase observations from m satellites on the same f frequencies, the sizes of the main matrices and vectors defined in this paper are given in Table A-1.

TABLE A-1
Notation and Sizes of Main Vectors and Matrices

Symbol	size	comment
$p_{r,f}$	$(m-1)\times 1$	SD code observations of antenna r, frequency f
$\varphi_{r,f}$	$(m-1)\times 1$	SD phase observations of antenna 1, frequency f
P_r	$f(m-1)\times 1$	SD code observations of antenna r
Φ_r	$f(m-1)\times 1$	SD phase observations of antenna r
y_r	$2f(m-1)\times 1$	All SD observations of antenna r
$y_{P_{12}}$	$f(m-1)\times 1$	DD code observations of antennae 1 and 2
$y_{\Phi_{12}}$	$f(m-1)\times 1$	DD phase observations of antennae 1 and 2
Y	$2f(m-1)\times(a-1)$	All DD observations of the array
$vec[y_r, Y]$	$2f(m-1)a\times 1$	Observation set of the A-POAD model
$vec(Y_r)$	$2f(m-1)a\times 1$	All SD observations in *vec* form
g_r^s	3×1	Unit-direction vector to satellite s
$G=G_r$	$2f(m-1)\times 3$	Geometry component of the design matrix
A	$2f(m-1)\times f(m-1)$	Ambiguity component of the design matrix
Q_p	$m\times m$	Covariance matrix of undifferenced code observations
Q_ϕ	$m\times m$	Covariance matrix of undifferenced phase observations
$Q_{y_{P_{12}}}$	$(m-1)\times(m-1)$	Covariance matrix of DD code observations
$Q_{y_{\Phi_{12}}}$	$(m-1)\times(m-1)$	Covariance matrix of DD phase observations
Q_r	$a\times a$	Covariance matrix of the array (array precision)
Q_f	$f\times f$	Contribution of frequencies
$Q_{vec[y_r,Y]}$	$2f(m-1)a\times 2f(m-1)a$	Covariance matrix of the A-POAD model
Q_Y	$2f(m-1)(a-1)\times 2f(m-1)(a-1)$	Covariance matrix of DD observations
z_r	$f(m-1)\times 1$	All SD observations of antenna r
Z	$f(m-1)\times(a-1)$	All DD observations of the array
B	$3\times(a-1)$	All baselines (considering one antenna as reference)
∇	$(m-1)\times 2m$	DD operator
D_i^T	$(i+1)\times i$	Differencing matrix
e_i	$1\times i$	Row vector with elements equal to 1
I_i	$i\times i$	Identity matrix
c_1	$(i+1)\times 1$	Column vector in which the first element equals 1 and the remainder equal 0